JOURNAL OF MECHANICAL ENGINEERING AND SCIENCES
ISSN: 2289-4659 e-ISSN: 2231-8380
VOLUME 20, ISSUE 1, 2026, 11052 - 11059
DOI: https://doi.org/10.15282/jmes.20.1.2026.3.0863

RESEARCH ARTICLE

Cyclic hardening and softening of high-strength steels

Norhaida Ab Razak*, Nasrul Azuan Alang, Nurizzatul Atikha Rahmat

Faculty of Mechanical and Automotive Engineering Technology, Universiti Malaysia Pahang Al-Sultan Abdullah, 26600 Pekan, Pahang, Malaysia

Abstract - 316L and P91 steels, commonly used for high-temperature applications in power plants, experience low-cycle fatigue. In this work, the cyclic stress-strain behaviour of 316L and P91 materials was analyzed. Experimental data from the material's hysteresis loops and cyclic stress response were used to derive material parameters for numerical simulation of the cyclic behaviour. The displacement-controlled model with strain amplitudes of 0.4% and 0.6% and a constant strain rate of 0.001 s^{-1} was used in the simulation. The simulation results show that 316L stainless steel exhibits cyclic hardening, with the maximum stress increasing from 311.3 MPa in the first cycle to 354.7 MPa at the half-cycle, corresponding to approximately 14% cyclic hardening. In contrast, P91 steel exhibits cyclic softening of about 8.3%, as the stress decreases from 497.9 MPa in the first cycle to 456.7 MPa at the half cycle. The findings also demonstrated that tension and compression loadings with larger strain amplitudes produced higher maximum stress. It also demonstrates that higher strain amplitudes result in a greater decrease in stress near the half cycle because hardening/softening is more pronounced at higher strain amplitudes.

Article History
Received : 28 September 2025
Revised : 31 January 2026
Accepted : 27 February 2026
Published : 31 March 2026

Keywords
Low-cycle fatigue
Cyclic softening
Cyclic hardening

1. Introduction

The growth of global industries, such as power plants, drives the development of new steel types. P91 steel is a martensitic steel, whereas 316L is an austenitic steel; both steels have high thermal resistance and thermal conductivity, enabling them to be widely used in high-temperature environments such as boilers, turbines, and power plants [1-2]. During these services, components are exposed to cyclic mechanical and thermal loading, leading to thermomechanical fatigue damage. Various experimental studies have analyzed the effect of cyclic loading conditions on the material's cyclic stress-strain behaviour. Cyclic hardening and cyclic softening behaviour will develop during exposure to cyclic loading conditions. Cyclic hardening behaviour occurs when the material's stress amplitude increases with the number of cycles during cyclic loading at constant strain amplitude. In contrast, cyclic softening behaviour occurred as cyclic stress amplitude decreased with cycle number under the same conditions, as illustrated in Figure 1 [3]. The behaviour of both is dependent on the material and the loading amplitude. Experimental studies have shown that 316L exhibits initial cyclic hardening followed by prolonged softening, whereas P91 material exhibits cyclic softening behaviour [4-7]. The relationship between maximum stress and the number of cycles differs between cyclic hardening and cyclic softening: in cyclic hardening, the maximum stress increases with the number of cycles. In contrast, cyclic softening is characterized by a decrease in the maximum stress with increasing cycles, as is typical for P91. The material's softening rate is directly proportional to the strain amplitude, indicating that the strain amplitude influences the material's cyclic stress response [6]. Numerical simulation can be used as an alternative method to evaluate cyclic behaviour and predict material damage. The finite element model used to simulate low-cycle behaviour employed the Prager model [8], the Armstrong-Frederick model [9], and the Chaboche model [10-11]. The Chaboche model is often used in finite element software [12-13]. The model contains a large number of material constants and variables that must be calibrated to produce predictions comparable to experimental results [14].

Recent studies have highlighted the importance of advanced modeling strategies for accurate fatigue prediction under cyclic loading. Subasic et al. [15] developed a constitutive model to analyse the cyclic plasticity for modelling additively manufactured 316L stainless steel, capturing the full hysteresis loop to improve fatigue life prediction. Cho et al. [16] proposed a numerical model that accurately simulates the cyclic behavior of high-strength steel, accounting for its peculiar material behavior and low-cycle fatigue. A physics-based crystal plasticity finite element method was used to investigate the microstructural response of high-strength steel to various loading types, revealing correlations between morphology, dislocation density, and deformation response under different loading conditions [17]. Although numerous studies have documented the cyclic response of austenitic and martensitic steels experimentally, comparatively few have leveraged stabilized-cycle data directly in constitutive FE modeling to enhance predictive capability. Integrating this stabilized data improves calibration of material models, reduces reliance on extrapolation from primary cycles, and enhances fatigue life prediction accuracy, particularly for 316L and P91 steels. In this work, the direct method of using the test data is employed. These can be achieved by using the stabilized cycle. The material parameters required to model the cyclic behaviour in the numerical simulation were derived from the material's hysteresis loops and cyclic stress response. The material model is then used to simulate the cyclic hardening and softening behaviour of 316L and P91 steels, respectively.

*CORRESPONDING AUTHOR | N.A. Razak | ✉ norhaida@umpsa.edu.my

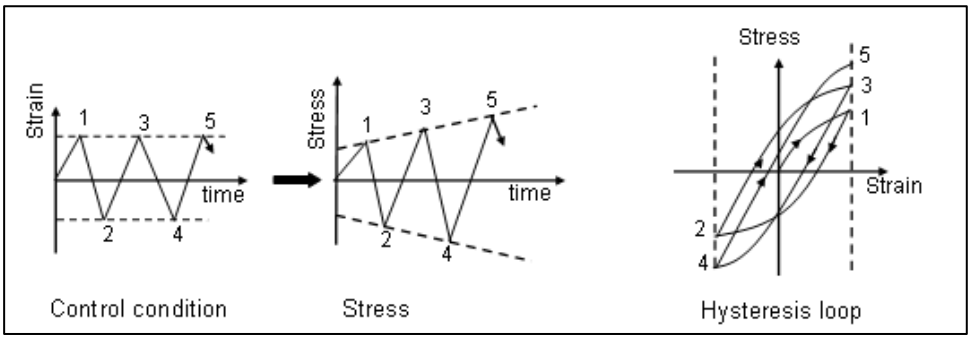

(a) cyclic hardening

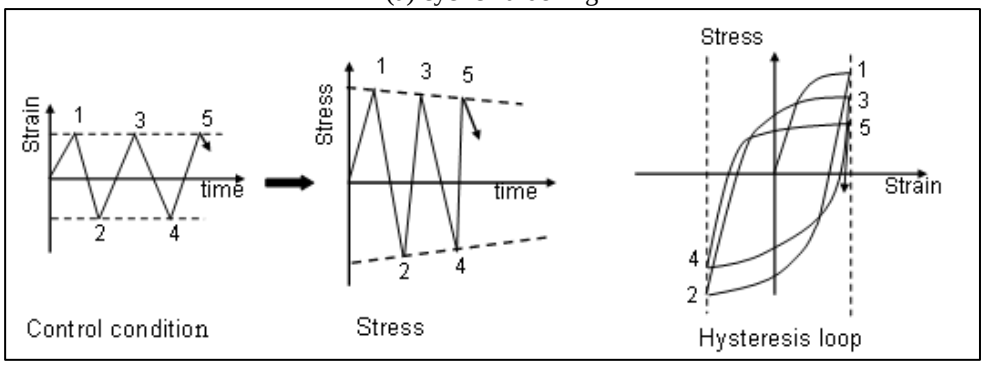

(b) cyclic softening

Figure 1. Illustration of cyclic response of cyclic hardening and cyclic softening [3]

2. Materials and Methods

2.1 Materials

Table 1 tabulates the tensile properties of P91 steel and 316L austenitic stainless steel at room temperature based on literature data [7, 18]. The yield strength and tensile strength of P91 martensitic steel are greater than those of 316L austenitic stainless steel.

Table 1. Tensile properties of P91 [7] and 316L [18] steels

Material	Temp (°C)	σ_{YS} (MPa)	σ_{UTS} (MPa)	E(GPa)	Poisson's ratio
P91	25	570	663	203	0.30
316L	25	211	515	200	0.28

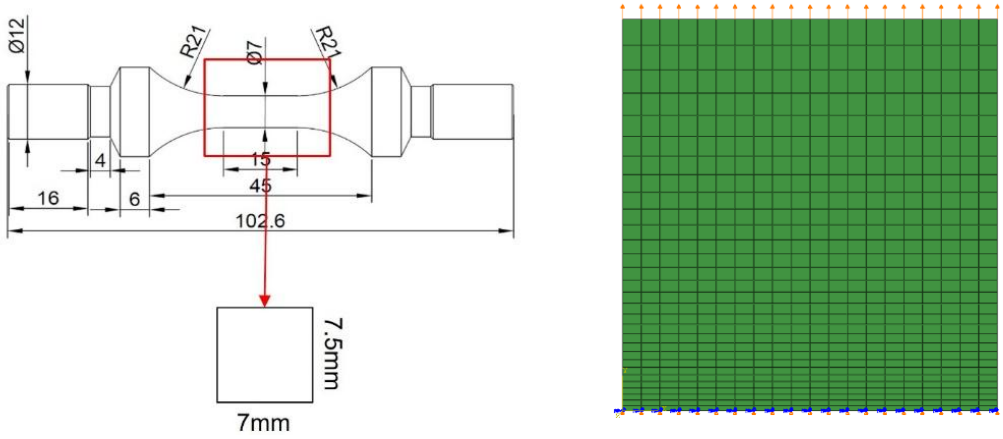

(a) Specimen b) Mesh and boundary conditions

Figure 2. Finite element model

2.2 Finite Element Modelling

ABAQUS software v6.14 was used to simulate cyclic loading of the material [19]. The specimen was modelled in ABAQUS using four-node CAX4R elements and a nonlinear, isotropic kinematic hardening model. CAX4R elements are used due to the axisymmetric geometry and loading conditions, providing an efficient and accurate simulation of

cyclic stress–strain behavior, while reduced integration minimizes shear and volumetric locking. Only half of the specimen's cross-sectional plane was modelled, as shown in Figure 2(a), due to the specimen's axisymmetric shape, to reduce computational effort in the analysis. The boundary conditions were applied at the bottom nodes of the model, constrained in the *y*-direction. The displacement-controlled load is applied to the desired strain amplitude at the upper nodes of the specimen, as shown in Figure 2(b). The strain rate employed was 1×10^{-3} s^{-1} and the strain amplitudes used were 0.4% and 0.6%. The material model parameters for the finite element analysis are extracted from the experimental study on P91 steel [7] and from literature data for 316L austenitic stainless steel [18]. Based on the experimental results for P91 steel, the data collected at the highest strain amplitude (0.6%) are used to develop the material model.

2.3 Determination of Model Parameters

Material under cyclic loading conditions undergoes plastic deformation, with cyclic softening or hardening. Cyclic stress-strain behaviour can be represented by combining the nonlinear isotropic and kinematic hardening models based on experimental data. Kinematic and isotropic hardening components can be calculated using Chaboche's material model parameters [20]. This Chaboche model contains a large number of material constants and variables that must be calibrated to yield predictions comparable to experimental results. Therefore, a direct method for utilising test data from a stabilized cycle is proposed, in which each data point for stress and strain must be specified.

2.3.1 Kinematic hardening components

By employing the direct method, the kinematic hardening component for the material model can be defined using the stabilized cycle of the hysteresis loop in the experimental data. The stabilised cycle is the cycle in which the model reaches a steady state, as the hysteresis loop shape no longer changes from one cycle to the next. Figure 3 shows the schematic of a hysteresis loop for a stabilized cycle.

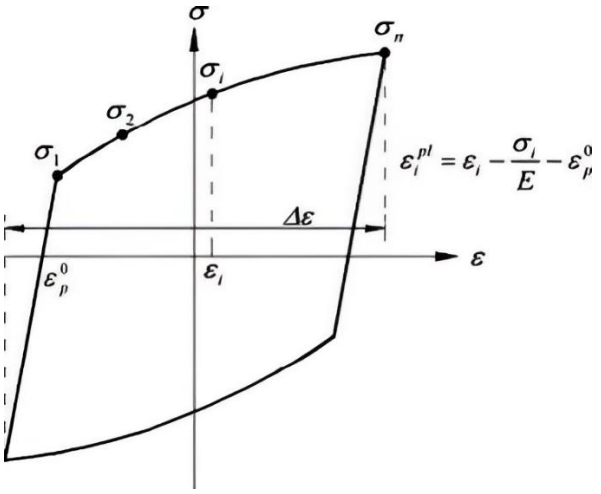

Figure 3. Hysteresis loop data for a stabilized cycle [19]

The kinematic hardening parameter can be obtained by fitting data pairs of stress and plastic strain $(\sigma_i, \varepsilon_i^{pl})$ of the stabilized hysteresis loop [19]. The plastic strain is calculated by shifting the initial plastic strain, ε_{pl}^0, where it crosses the strain axis, as shown in Figure 3, where the plastic strain is calculated as Eq. (1).

$$\varepsilon_i^{pl} = \varepsilon_i - \frac{\sigma_i}{E} - \varepsilon_p^0 \tag{1}$$

As the initial data pair will be denoted as $(\sigma_1, 0)$, where the initial plastic strain is zero. The value of backstress of each data pair can be calculated by the difference of stress with the stabilised data of the yield surface, $(\sigma_1 + \sigma_n)/2$, as shown in Figure 3.

$$\alpha_i = \sigma_i - \frac{\sigma_i - \sigma_n}{2} \tag{2}$$

The back-stress value obtained in Equation 2, α_i, is the overall sum of all backstress obtained at this data point. At this uniaxial strain cycle, the backstress evolution laws are integrated with the exact match of the first data pair, which brings the expression

$$\alpha_k = \frac{C_k}{\gamma_k}\left(1 - e^{\gamma_k \varepsilon^{pl}}\right) + \alpha_{k,1} e^{\gamma_k \varepsilon^{pl}} \tag{3}$$

2.3.2 Isotropic hardening components

Isotropic hardening components can be obtained by specifying the equivalent stress, σ^n, which is defined as the size of the yield surface (elastic range), as a tabular function of equivalent plastic strain, $\bar{\varepsilon}^{pl}$. The hardening/softening behaviour of a material can be estimated using the data pair of equivalent stress and equivalent plastic strain (σ^n,$\bar{\varepsilon}^{pl}$) from the hysteresis loop. The symmetric plastic strain cycle from experimental data is illustrated as shown in Figure 4 for a typical hardening behaviour of a material.

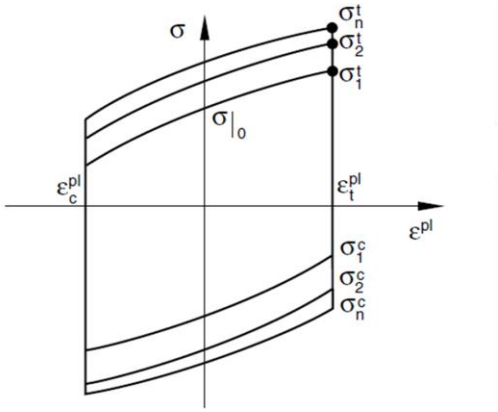

Figure 4. Plastic strain cycle with hardening behaviour [19]

The equivalent stress or the yield surface can be calculated using the maximum tensile stress, σ_i^t, and the maximum compression stress, σ_i^c, in the elastic range, such that

$$\sigma_i^0 = \sigma_i^t - \alpha_i \tag{4}$$

$$\alpha_i = \frac{\sigma_i^t - \sigma_i^c}{2} \tag{5}$$

where α_i, is the backstress, which can be calculated by Eq. (5) as it can be obtained by separating the kinematic component from the yield stress of the hysteresis loop. The equivalent plastic strain can be calculated using the plastic strain range, as shown in Figure 4.

$$\Delta\varepsilon^{pl} = \varepsilon_t^{pl} - \varepsilon_c^{pl} \tag{6}$$

where the ε_t^{pl} and ε_c^{pl} are the maximum plastic strains in tension and compression, respectively. The equivalent plastic strain was set to zero, so the material's yield strength determines the initial yield surface. The equivalent plastic strain corresponding to the other stress can be expressed by Eq. (7).

$$\bar{\varepsilon}_i^{pl} = \frac{1}{2}(4i-3)\Delta\varepsilon^{pl} \tag{7}$$

The hysteresis loop has imperfections, so the strain data slightly exceeds the hysteresis curve's strain range. This can be adjusted by using a straight line with an offset parallel to the slope of Young's modulus of a cycle to determine the elastic range of the hysteresis loop. This can be used to estimate better the elastic range of the material's hysteresis loop from experimental data.

3. Results and Discussion

Cyclic stress-strain behaviour, also known as the hysteresis loop, can be represented by a combination of nonlinear isotropic and kinematic hardening models. The isotropic and kinematic hardening components of the material model can be defined from the stabilised hysteresis loop in the experimental data using the direct method. In this work, the material model parameters for the finite element analysis are extracted from an experimental study of P91 steel [7] and from literature data for 316L austenitic stainless steel [18]. Based on the experimental results for P91 steel, the data collected at the highest strain amplitude (0.6%) are used to develop the material model. The comparison of experimental and simulation results for P91 steel is presented in previous work [21], which demonstrates a strong correlation between the two. The percentage deviation between simulated and experimental stress amplitudes was calculated using the first and stabilized cycle. For both materials, the deviation was within ±4%, indicating good agreement between the numerical predictions and experimental observations and confirming that the calibrated cyclic plasticity parameters effectively capture the stabilized cyclic response of both austenitic and martensitic steels.

Figure 5 shows the simulated cyclic stress-strain behaviour of 316L steel and P91 steel at the first cycle and half-cycle for the strain amplitude of 0.6%. The stress amplitude increases with the number of cycles for 316L steel (Figure 5(a)), where the maximum stress increases from 311.29 MPa in the first cycle to 354.69 MPa in the half cycle, indicating that 316L exhibits cyclic hardening. P91 material undergoes cyclic softening as the number of cycles increases, as the stress

amplitude of the material decreases from 497.87 MPa in the first cycle to 456.7 MPa in the half cycle, as shown in Figure 5(b).

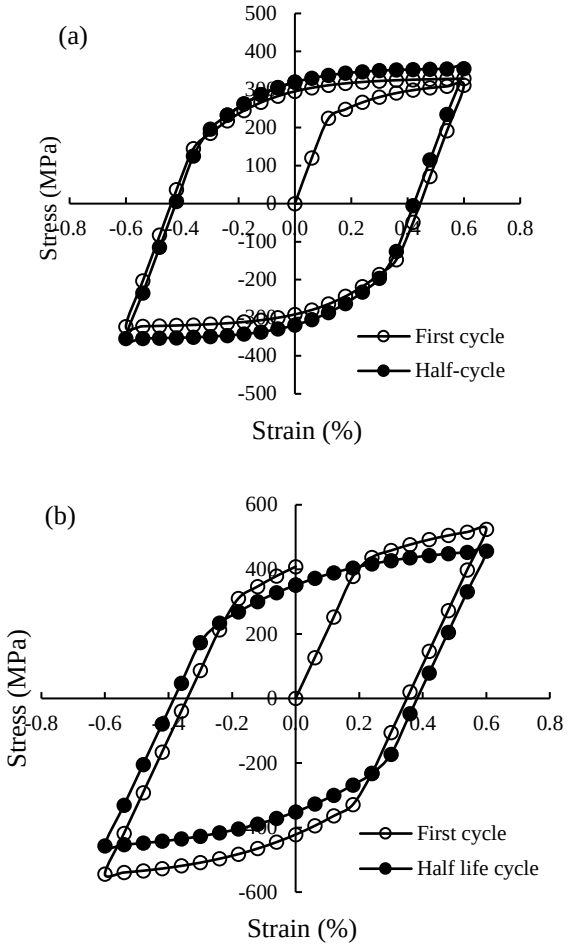

Figure 5. Hysteresis loop first cycle and half cycle (a) 316L steel; (b) P91

The hysteresis loops for 316L and P91 steel are shown in Figure 6 for 0.4% and 0.6% strain amplitude. The simulation's findings indicate that 316L exhibits cyclic hardening at a strain amplitude of 0.4%, with stress rising from the first to the half-cycle. In contrast, cyclic softening occurs in the P91 hysteresis loop at 0.4% strain amplitude. The results showed that larger strain amplitudes under tension and compression loading led to higher maximum stress. It also demonstrates that higher strain amplitudes result in a greater decrease in stress near half cycle because softening is more pronounced at higher strain amplitudes. Figure 7 shows the cyclic stress behaviour of P91 and 316L at strain amplitudes of 0.4% and 0.6%. The P91 steel exhibits cyclic softening, with an initial peak stress of 497.87 MPa in the first cycle, compared to 474.97 MPa at the 50th cycle. As for the 316L steel, it exhibits cyclic hardening, with the peak stress increasing from 311.29 MPa in the first cycle to 354.69 MPa in the 50th cycle. Several factors determine the cyclic behaviour of a material. Srinivasan et al. reported that 316L stainless steel undergoes initial hardening to a maximum stress, followed by a stable peak stress, which marks the stabilized cycle, and then a rapid drop in stress due to dynamic strain aging [22]. The cyclic hardening in 316L is attributed to the effects of mutual interaction among dislocations, where fine precipitates are formed in the dislocations during plastic deformation [2]. The degree of hardening of material 316L is found to be dependent on the strain amplitude, as the hardening increases with an increase in strain amplitude [18]. As for P91 steel, cyclic softening occurs due to microstructural evolution within the specimen, leading to a rapid, nonlinear decrease in peak stress. This is followed by the initiation of cracks and microstructural changes in the material before crack propagation and failure [23]. The cyclic softening behaviour is associated with the transformation of the original martensite lath structure into a dislocation cell structure and greatly affects the fatigue life of the material [24],[25]. Cyclic softening-related fractures need to be carefully monitored because they can significantly compromise the structural integrity of components and shorten their operational life. The observed cyclic hardening and softening behaviors have important implications for fatigue life prediction and structural component design. Cyclic hardening, as observed in 316L, can lead to increased stress amplitudes during early service life, potentially accelerating crack initiation under strain-controlled conditions. In contrast, cyclic softening in P91 may result in localized strain accumulation, increasing susceptibility to ratcheting and premature failure under cyclic loading. Incorporating stabilized cyclic behavior into FE simulations enables more realistic stress–strain predictions, thereby improving fatigue life assessment and supporting safer, more reliable component design in high-temperature, cyclic service environments.

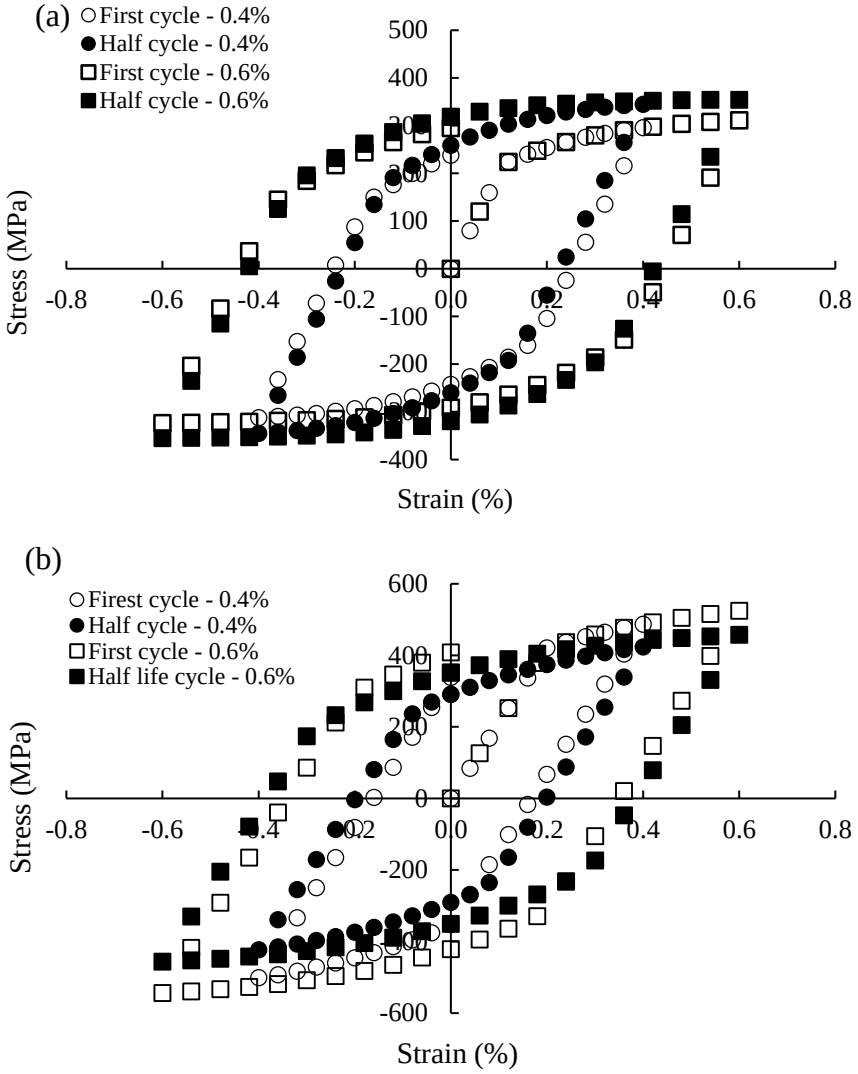

Figure 6. Hysteresis loop of 0.4% vs 0.6% strain amplitude (a) 316L steel; (b) P91

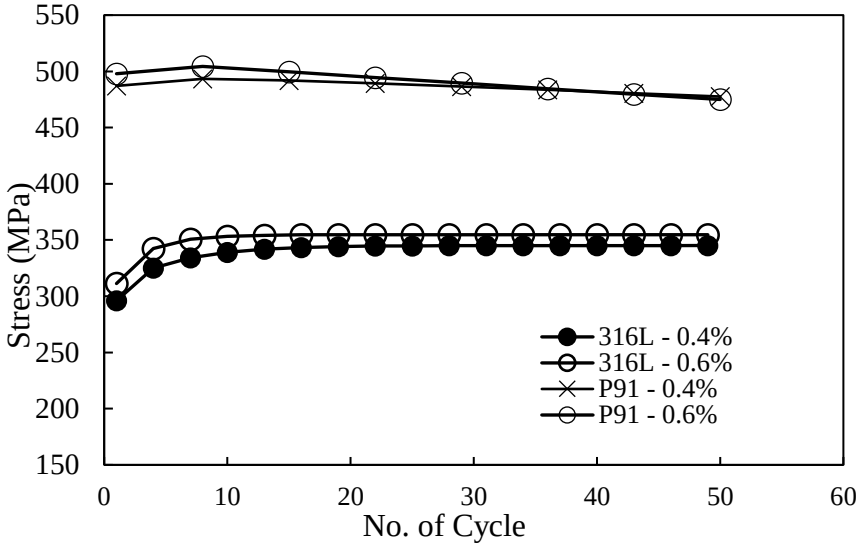

Figure 7. Cyclic stress response of P91 and 316L for 0.4% and 0.6% strain amplitude

4. Conclusions

This study demonstrates that the cyclic deformation behaviour of both 316L and P91 steels can be accurately represented numerically. The simulation results show that 316L stainless steel exhibits cyclic hardening, with the maximum stress increasing from 311.3 MPa in the first cycle to 354.7 MPa at the half-cycle, corresponding to approximately 14% cyclic hardening. In contrast, P91 steel exhibits cyclic softening of about 8.3%, as the stress decreases from 497.9 MPa in the first cycle to 456.7 MPa at the stabilized cycle. The distinct cyclic responses observed for the two materials have important implications for fatigue performance and structural integrity under service conditions. In particular, the numerical approach provides a reliable basis for constitutive model calibration and can support finite element simulations of power plant components, such as steam pipes and pressure vessels, operating under cyclic and high-temperature loading conditions.

Acknowledgements

The authors gratefully acknowledge Universiti Malaysia Pahang Al-Sultan Abdullah, and the Faculty of Mechanical and Automotive Engineering Technology for providing the laboratory facilities that enabled this work.

Funding

This study was not supported by any grants from funding bodies in the public, private, or not-for-profit sectors.

Declaration of Competing Interest

The author declares no conflicts of interest.

CRediT Authorship Contribution Statement

Norhaida Ab Razak (Conceptualisation; Data curation, Formal analysis; Visualisation; Writing – original draft)
Nasrul Azuan Alang (Methodology; Formal analysis; Writing – review and editing)
Nurizzatul Atikha Rahmat (Writing – review and editing)

Availability of Data and Materials

The data supporting this study's findings are available on request from the corresponding author.

Ethics Declarations

This study did not involve human participants or animals. Ethical approval was therefore not required.

Generative Artificial Intelligence Declarations

The authors stated that generative AI was not used to generate content, ideas, or theories. We have just utilised AI to enhance readability and refine the language. This was used with extreme human control and oversight. The authors take full responsibility for reviewing and approving the content.

References

[1] A. Shibli and F. Starr, "Some aspects of plant and research experience in the use of new high-strength martensitic steel P91," *International Journal of Pressure Vessels and Piping*, vol. 84, no. 1, pp. 114–122, 2007.

[2] V. Shankar, K. Mariappan, R. Sandhya, and K. Laha, "Understanding low cycle fatigue and creep–fatigue interaction behavior of 316 L(N) stainless steel weld joint," *International Journal of Fatigue*, vol. 82, pp. 487–496, 2016.

[3] D. W. Hoeppner, "Cyclic Loading and Cyclic Stress," in *Encyclopedia of Tribology*, Q. J. Wang and Y.-W. Chung, Eds., Boston, MA: Springer US, 2013, pp. 691–698.

[4] V. S. Srinivasan, M. Valsan, R. Sandhya, K. Bhanu Sankara Rao, S. L. Mannan, and D. H. Sastry, "High temperature time-dependent low cycle fatigue behaviour of a type 316L(N) stainless steel," *International Journal of Fatigue*, vol. 21, no. 1, pp. 11–21, 1999.

[5] L. Zhao, Y. Song, L. Xu, Y. Han, and K. Hao, "Investigation of the high-temperature low-cycle fatigue failure characteristics of p91 steel weld joints and their fatigue strength reduction factors under various load control regimes," *International Journal of Fatigue*, vol. 180, p. 108085, 2024.

[6] G. Golański and S. Mroziński, "Low cycle fatigue and cyclic softening behaviour of martensitic cast steel," *Engineering Failure Analysis*, vol. 35, pp. 692–702, 2013.

[7] N. A. A. Razak, *Creep and creep fatigue interaction in new and service-exposed P91 steel*. Imperial College London, 2018. [Online]. Available: https://books.google.com.my/books?id=_D7vzQEACAAJ

[8] W. Prager, "A new method of analyzing stresses and strains in work-hardening plastic solids," *Journal of Applied Mechanics*, vol. 23, no. 4, pp. 493–496, 2021.

[9] A. F. Fossum, "Parameter estimation for an internal variable model using nonlinear optimization and analytical/numerical response sensitivities," *Journal of Engineering Materials and Technology*, vol. 119, no. 4, pp. 337–345, 1997.

[10] J. L. Chaboche and G. Rousselier, "On the Plastic and Viscoplastic Constitutive Equations—Part I: Rules Developed with Internal Variable Concept," *Journal of Pressure Vessel Technology, Transactions of the ASME*, vol. 105, no. 2, pp. 153–158, 1983.

[11] J. L. Chaboche and G. Rousselier, "On the plastic and viscoplastic constitutive equations- Part II: Application of internal variable concepts to the 316 stainless steel," *Journal of Pressure Vessel Technology, Transactions of the ASME*, vol. 105, no. 2, pp. 159–164, 1983.
[12] G. Dundulis, R. Janulionis, A. Grybėnas, V. Makarevičius, and R. Dundulis, "Numerical and experimental investigation of low cycle fatigue behaviour in P91 steel," *Engineering Failure Analysis*, vol. 79, pp. 285–295, 2017.
[13] B. Das, A. Bakkar, N. Khutia, and D. Das, "Low cycle fatigue performance evaluation of TMT rebar," *Materials Today: Proceedings*, vol. 4, no. 2, Part A, pp. 2554–2563, 2017.
[14] P. Kubaschinski, A. Gottwalt, U. Tetzlaff, H. Altenbach, and M. Waltz, "Calibration of a combined isotropic-kinematic hardening material model for the simulation of thin electrical steel sheets subjected to cyclic loading," *Materwiss. Werksttech.*, vol. 53, no. 4, pp. 422–439, 2022.
[15] M. Subasic, A. Ireland, R. Mansour, P. Enblom, P. Krakhmalev, M. Åsberg et al., "Experimental investigation and numerical modelling of the cyclic plasticity and fatigue behavior of additively manufactured 316 L stainless steel," *International Journal of Plasticity*, vol. 176, p. 103966, 2024.
[16] E. Cho and S. W. Han, "A numerical model simulating cyclic behavior of high-strength steel," *Advances in Structural Engineering*, vol. 27, no. 9, pp. 1490–1508, 2024.
[17] M. H. Joudivand Sarand and I. B. Misirlioglu, "A physics-based plasticity study of the mechanism of inhomogeneous strain evolution in dual phase 600 steel," *International Journal of Plasticity*, vol. 174, p. 103918, 2024.
[18] S. C. Roy, S. Goyal, R. Sandhya, and S. K. Ray, "Low cycle fatigue life prediction of 316 L(N) stainless steel based on cyclic elasto-plastic response," *Nuclear Engineering and Design*, vol. 253, pp. 219–225, 2012.
[19] Abaqus, "Abaqus models for metals subjected to cyclic loading," 2016.
[20] J. L. Chaboche, "Time-independent constitutive theories for cyclic plasticity," *International Journal of Plasticity*, vol. 2, no. 2, pp. 149–188, 1986.
[21] M. A. A. Roslin, N. Ab Razak, N. A. Alang, and N. Sazali, "Numerical simulation of P91 steel under low-cycle-fatigue loading," *Journal of Failure Analysis and Prevention*, vol. 23, no. 2, pp. 520–528, 2023.
[22] V. S. Srinivasan, R. Sandhya, K. Bhanu Sankara Rao, S. L. Mannan, and K. S. Raghavan, "Effects of temperature on the low cycle fatigue behaviour of nitrogen alloyed type 316L stainless steel," *International Journal of Fatigue*, vol. 13, no. 6, pp. 471–478, 1991.
[23] B. Fournier, F. Dalle, M. Sauzay, J. Longour, M. Salvi, C. Caës et al., "Comparison of various 9–12%Cr steels under fatigue and creep-fatigue loadings at high temperature," *Materials Science and Engineering: A*, vol. 528, nos. 22–23, pp. 6934–6945, 2011.
[24] S. K. Basantia, A. Bhattacharya, N. Khutia, and D. Das, "Plastic behavior of ferrite–pearlite, ferrite–bainite and ferrite–martensite steels: Experiments and micromechanical modelling," *Metals and Materials International*, vol. 27, no. 5, pp. 1025–1043, 2021.
[25] P. Lehner, B. Blinn, and T. Beck, "Changes in microstructure and mechanical properties of ferritic high chromium steel and P91 induced by isothermal fatigue," *Materials Science and Engineering: A*, vol. 923, p. 147713, 2025.